Hyperspectral Unmixing: A critical comparison

Spandana Ettireddy
Vasavi College of Engineering
Hyderabad, India
spandanaettireddy@gmail.com

Sree Nithya Panduga
Vasavi College of Engineering
Hyderabad, India
sreenithyapanduga27@gmail.com

Srijani Mekala
Vasavi College of Engineering,
Hyderabad, India
srijani0910@gmail.com

Dr. T Hitendra Sarma
Vasavi College of Engineering
Hyderabad, India
hitendrasarma@staff.vce.ac.in

***Abstract*—Hyperspectral imaging (HSI) has developed as an important method in remote sensing, providing comprehensive spectral data for each pixel in an image. However, HSI's limited spatial resolution frequently results in mixed signals from several materials inside a single pixel, creating a considerable barrier for hyperspectral unmixing (HU). In HU, the aim is to determine the spectra of endmembers and their abundances in each pixel, which is complicated by noise, atmospheric influences, and spectral variation. Deep learning approaches, notably autoencoders, have demonstrated promise in tackling these issues by developing efficient representations of hyperspectral data.This research gives a detailed evaluation of autoencoder-based HU methods, with a focus on blind unmixing approaches.**

Datasets are critical in determining the performance of HU techniques The datasets include Cuprite, Jasper Ridge, and Urban, each representing different environments and material compositions commonly encountered in HSI applications.

To develop and compare deep unmixing autoencoders, we use popular deep learning packages like TensorFlow/Keras. These packages offer a flexible and effective framework for creating and training neural network models. Furthermore, crucial Python libraries such as NumPy, SciPy, and Matplotlib are used for data manipulation, scientific computation, and visualization, respectively. Using these libraries, we hope to conduct a complete evaluation of autoencoder-based approaches, evaluating their performance, accuracy, reconstruction error, and mean spectral angle distance (mSAD) across multiple datasets.Through our testing and analysis, we hope to provide insights into the strengths and limits of various autoencoder architectures for HU, guiding researchers and practitioners in selecting appropriate approaches for their particular applications.

***Index Terms*—Hyperspectral unmixing, endmember extraction, auto-encoders, abundances, Mean spectral angle distance.**

I. Introduction

In the realm of data-intensive fields like hyperspectral imaging, the advent of deep learning (DL) has ushered in a new era of possibilities. Hyperspectral imaging, a subset of imaging spectrometry, captures an entire spectrum at every pixel, rendering its data highly dimensional and large compared to other imaging techniques. The high spectral resolution inherent in hyperspectral images (HSIs) enables the identification of pure materials, or end members, present in a scene. However, due to the low spatial resolution, individual pixels often encompass multiple end members. Consequently, determining the spectra of these end members and their proportions within each pixel—a process known as hyperspectral unmixing (HU)—poses a formidable inverse problem. [1]

Traditionally, HU methods focus on extracting end members, leaving the determination of their abundances to subsequent steps using other techniques [2]. However, blind unmixing methods, which simultaneously ascertain both end members and their abundances, are gaining traction. Autoencoders, a class of neural networks, offer a versatile framework for unsupervised learning, making them well-suited for addressing the challenges of hyperspectral unmixing. [3] Their ability to capture complex relationships within data while simultaneously reducing dimensionality makes them a compelling choice for feature extraction and representation learning.

With a focus on blind approaches, this project aims to critically compare autoencoder-based algorithms for HU and provide a thorough understanding of various autoencoder architectures. The studies will mostly focus on blind methods, while admitting the availability of non-blind ways using DL techniques. By exploring the strengths and limitations of each architecture and methodology, a nuanced understanding of their applicability in HU tasks will be developed. Moreover, the project will highlight the significance of utilizing both synthetic and real datasets in the evaluation process. Synthetic datasets allow for controlled experimentation and benchmarking, while real datasets offer insights into the complexities and nuances present in practical applications. Furthermore, the project will explore the intersection of autoencoder-based methods with other DL techniques, such as convolutional neural networks (CNNs) to harness their complementary strengths in hyperspectral unmixing tasks. [4]

By providing a critical comparison of autoencoder-based methods for HU, this project aims to address key research questions regarding their effectiveness, efficiency, and scalability. Insights gained from this endeavor will not only advance the state-of-the-art in hyperspectral imaging analysis but also facilitate the development of innovative solutions for real-world challenges in fields like remote sensing, environmental monitoring, and biomedical imaging. Through dissemination

of findings via scholarly publications and presentations, the project aims to contribute to the broader scientific community and inspire further research in this exciting and rapidly evolving domain.

The project uses Deep Unmixing methods; CNN, DAE(Deep unmixing autoencoder), SIDAEU, OSPAEU, mDAE, MTLAEU for HU. Based on mSAD and reconstruction error of these methods we compare the performance of these methods and find out the best method for hyperspectral unmixing.

II. Literature Survey

A thorough analysis of nonlinear hyperspectral unmixing techniques may be found in the [5]. It explores methods for identifying and isolating the constituent materials found in hyperspectral imaging, taking into consideration intricate nonlinear mixing events. It has different methods and algorithms used in nonlinear unmixing and point out their advantages, disadvantages, and uses. The focus is on improvements in nonlinear spectral unmixing techniques, which tackle issues including endmember variability, nonlinearity, and spectral variability. The theoretical underpinnings, mathematical formulations, and real-world applications of nonlinear unmixing algorithms in remote sensing applications are examined in this work.

The study by [6], offers a thorough description of hyperspectral unmixing methods. It concentrates on three primary areas: statistical, geometrical, and sparse regression-based methods.The mathematical models and algorithms for unmixing hyperspectral imagery—which take into account both linear and nonlinear mixing scenarios—are emphasized. The paper tackles issues like accuracy of abundance estimation, variability of endmembers, and spectral variability. It also investigates how to enhance unmixing performance by integrating extra limitations and past knowledge.

In [7], it mainly address endmember variability in hyperspectral analysis. It looks into methods to take spectral variability into account and lessen it during spectral unmixing procedures. The authors talk about how endmember variability affects spectral unmixing algorithms' accuracy and how this affects applications in distant sensing. The focus is on creating strong techniques that can handle various spectral fingerprints in a scene. To successfully handle endmember variability, the research investigates data-driven techniques, optimization strategies, and statistical models. It offers explanations of the difficulties caused by endmember variability and suggests fixes to raise the accuracy of hyperspectral analysis. All things considered, the work advances our knowledge of and ability to use spectral unmixing in real settings.

Along with [7], The review of endmember variability in spectral mixture analysis (SMA) [8] also focuses on endmember variability in HU. Its main goal is to investigate how the accuracy of SMA results is affected by variability in endmembers, or the pure spectral signatures that reflect the materials in a scene. The authors talk about how different endmember variability sources, such as spectral, temporal, and spatial parameters, affect SMA outputs. Understanding endmember variability's sources and how they affect remote sensing applications is emphasized. This research examines various ways for characterizing and reducing endmember variability, including statistical methods, spectral library building, and spectral angle mapper (SAM) techniques.

III. Methodology

A. Algorithm

1) Preprocessing:

a) Load HSI Data: Load the Hyperspectral Image (HSI) data from the dataset using the`load_HSI` function. Hyperspectral dataset X of dimensions N×M×L, where N is the number of pixels, M is the number of spectral bands, and L is the number of pixels. Normalize Data: Normalize the loaded data to a common scale. Function: Normalize X to have zero mean and unit variance across each spectral band.

$$Formula : X_{\text{norm}} = \frac{X - \mu_i}{\sigma}$$

where μ is the mean and σ is the standard deviation computed along each spectral band.

Extract Patches: Extract patches from the normalized HSI data for training

2) Auto-encoder Training:

a) Define Encoder: The encoder component is implicitly defined within the `create_model` method of the Autoencoder class. It includes layers such as Dense and Dropout for encoding the input data.

- The compression of input data is achieved through the layers defined within the encoder component.

- These layers, including dense and convolutional layers, perform transformations to compress the input data into a lower-dimensional latent representation.

- The output of the encoder component represents the latent representation or encoding of the input data.

b) Define Decoder: The decoder component is defined within the `create_model` method of the Autoencoder class.

- It includes layers such as Dense and Conv2D transpose for decoding the latent representation and reconstructing the original input data.

- The reconstruction of the input data is achieved through the layers defined within the decoder component.

- These layers perform transformations to expand the latent representation back into the original input space, reconstructing the input data.

The output of the decoder component represents the reconstructed input data.

3) Define loss function: Function: Train a deep autoencoder network with L input neurons, H hidden neurons, and L output neurons. Loss Function: Mean Squared Error (MSE)

$$Formula : MSE = \frac{1}{N} \sum_{i=0}^{N} |X_i - \hat{X}_i|^2$$

where:

$N =$ Number of data points

$X_i =$ Original data point at index i

$\hat{X}_i =$ Reconstructed data point at index i

4) Unmixing Process: Function: Use the trained autoencoder models to encode the observed mixed spectra into a lower-dimensional latent space representation.

Formula:

$$LatentRepresentation : Z = \text{Encoder}(X_{\text{norm}})$$

$$EstimatedAbundancefraction : A = Decoder(Z)$$

5) Evaluate Models:

a) Computational Complexity: Measure the number of parameters and operations required for training and inference.

b) Unmixing Accuracy: Compute RMSE or SAM between the ground truth and estimated abundance fractions.

IV. Experimental Study

This section provides the details of the datasets and the parameter setup for the current experimental study.

A. Datasets

Experiments are conducted on three datasets *viz.,* Cuprite, Jasper Ridge and Urban, which are popularly used to analyze the performance of hyperspectral unmixing techniques in the literature.

- **Urban:** Obtained by the Hyperspectral Digital Image Collection Experiment sensor [9], this image is 307 ×307 pixels and has 210 bands covering the 400–2500 nm wavelength range. After removing corrupted and noisy bands, 162 bands remain. Experiment is performed on this dataset for three times verifying different number of endmembers.
  1) Grass, Tree, Asphalt, and Roof were selected as the references for four endmembers.
  2) Grass, Tree, Asphalt, Soil and Roof were selected as the references for five endmembers.
  3) Grass, Tree, Asphalt, Soil, Metail and Roof were selected as the references for six endmembers.
- **Samson:**A basic dataset called Samson, there are 952 × 952 pixels in this picture. Every pixel has 156 channels recorded, spanning the wavelength range of 401 nm to 889 nm. Up to 3.13 nm, the spectral resolution is very excellent. A section of 95 × 95 pixels is utilized since the original image is too huge, which incurs significant computing costs. The original image's (252,332)-th pixel is where it begins. The blank channel or poorly noised channels do not impair this data. Three endmembers were chosen to have Tree, Water, and Soil as their references.
- **Jasper Ridge:** One well-known hyperspectral dataset is Jasper Ridge. It has 512 by 614 pixels. Every pixel is captured at 224 different wavelengths, spanning from 380 to 2500 nm. Up to 9.46 nm of spectral resolution is possible. As the hyperspectral image is too intricate to obtain the ground truth, we take into consideration a 100x100 pixel subimage. The original image's (105,269)-th pixel is where the first pixel begins. We are left with 198 channels after eliminating channels 1-3, 108-112, 154-166, and 220-224 (because of dense water vapor and atmospheric influences). Tree, Water, Soil, and Road were selected as the references for four endmembers.

B. Software Requirements

- TensorFlow/Keras for deep learning model development.
- IDE (Integrated Development Environment): Jupyter Notebook or Visual Studio Code or Google Colab.
- Deep Learning server

C. Analysis

TABLE I: mSAD(in Radians) FOR URBAN DATASET WITH 4 ENDMEMBERS

Endmemeber Method	Asphalt	Grass	Tree	Roof	Average
CNNAEU	0.0575	0.0366	0.0321	0.0332	0.0398
MITAEU	0.081	0.059	0.047	0.129	0.079
DAEU	0.050	0.073	0.044	0.201	0.092
DAEN	0.729	0.928	1.104	0.743	0.886
SIDAEU	0.069	0.130	0.045	0.382	0.157
OSPAEU	0.1290	0.0901	0.1350	1.2005	0.1386

TABLE II: mSAD(in Radians) FOR URBAN DATASET WITH 5 ENDMEMBERS

Endmemeber Method	Asphalt	Soil	Tree	Roof	Grass	Average
CNNAEU	0.0379	0.1075	0.1320	0.0404	0.0611	0.0708
MITAEU	0.1211	0.1652	0.1132	0.0661	0.0567	0.1044
SIDAEU	0.096	0.656	0.216	0.130	0.145	0.2486
OSPAEU	0.068	0.040	1.084	0.076	0.366	0.1268
DAEU	0.085	0.108	0.240	0.360	0.075	0.1736
DAEN	0.136	0.114	0.077	1.085	0.044	0.0912

TABLE III: mSAD(in Radians) FOR URBAN DATASET WITH 6 ENDMEMBERS

Endmemeber Method	Asphalt	Soil	Tree	Roof	Grass	Metal	Average
CNNAEU	0.043	0.103	0.133	0.043	0.049	0.362	0.122
MITAEU	0.142	0.360	0.037	0.108	0.072	0.073	0.132
SIDAEU	0.104	0.159	0.203	0.496	0.128	0.682	0.295
OSPAEU	0.068	0.338	0.091	0.071	0.081	0.042	0.185
DAEU	0.157	0.373	0.101	0.274	0.038	0.047	0.165
DAEN	0.313	0.557	0.903	0.498	0.796	0.526	0.599

- **Urban:** The first four, fifth, and sixth endmembers are extracted using the Urban dataset, and the extracted endmembers are compared to the reference endmembers. The difficulty of obtaining good solutions rises with the expected endmember count. Observing how the answers for the original endmembers change with the estimation of new endmembers is fascinating. Extracted endmembers for all techniques for the Urban dataset are displayed in Figure 1,3,5, where four, five, and six reference endmembers are used, respectively.CNNAEU,

MITAEU exhibit strong performance, low variation, and good accuracy when estimating four endmembers. The accuracy of the DAEN approach is poor, but consistency is good. The spectrum fluctuation in the image and the tying of the weights are probably the causes of the extreme instability of the mDAE method, which is the only method with tied weights. The mSAD score, or medium consistency and poor accuracy, are the characteristics of the DAEU and SIDAEU techniques. Because of the "Roof" endmember's oscillation between three alternative solutions, the OSPAEU approach has poor accuracy.

The accuracy of several approaches considerably drops as the number of estimated endmembers is increased to five, although the average SAD scores of all methods increase. Previously accurate endmembers start to become unsteady. Once more, CNNAEU, MITAEU exhibit the best accuracy and performance; CNNAEU has the best consistency and accuracy. In one inconsistent run, MTAEU estimates the Asphalt endmember as a "Tree" endmember variant, which leads to a lower consistency and worse mSAD.

The new "Soil" endmember is rather effectively estimated using the OSPAEU technique. The DAEN method had to be dropped because, for some reason, it was taking too long to extract six endmembers for this dataset.

TABLE IV: mSAD(in Radians) FOR SAMSON DATASET WITH 3 ENDMEMBERS

Endmemeber Method	Water	Soil	Tree	Average
CNNAEU	0.018	0.018	0.002	0.012
DAEU	0.020	0.046	0.042	0.036
DAEN	0.821	0.181	0.078	0.121
SIDAEU	0.108	0.121	0.326	0.185
OSPAEU	0.045	0.349	0.020	0.138
MITAEU	0.015	0.077	0.042	0.044

- **Samson:** Figure 7. displays the endmembers that were extracted using every technique for the Samson dataset. When it comes to this dataset, CNNAEU, MTAEU, and DAEU are the top three approaches.CNNAEU obtains the lowest average SAD score and demonstrates good accuracy as well, with only one run out of 25 producing a different solution for the "soil" endmember.There is a fair amount of consistency between the DAEU and SIDAEU techniques. Although mDAE is unreliable, it performs better on this dataset than it did on Urban. For the dataset, the MTAEU approach yields the second-lowest mSAD score.Overall, the Samson dataset exhibits less spectral variability with regard to scaling of spectra than the Urban dataset, as evidenced by the smaller performance gap between methods that employ and those that do not use scale-invariant fidelity terms.
- **JasperRidge:** The last dataset used to assess blind unmixing performance is called JasperRidge. Table V lists the average SAD scores for each endmember along with the mSAD score, and Fig. 9 displays all extracted endmembers for all techniques. The endmembers of this dataset are highly distinctive and simple to identify. Because the water spectra in this collection have a smaller scale than the other endmembers, working with the water endmember can be difficult. Extraction of such endmembers may prove challenging for methods relying on scale-sensitive similarity measurements, like mean square error (MSE). Removing the micro scale endmember and extracting a variation of a wellrepresented endmember will further reduce a scale-sensitive objective function. A badly learned endmember with anomalies and small scale can likewise appear as an endmember. The top three best methods are CNNAEU,MTAEU and DAEU.CNNAEU has the lowest mSAD score which results as the best method for this dataset.

TABLE V: mSAD(in Radians) FOR JASPER RIDGE DATASET WITH 4 ENDMEMBERS

Endmemeber Method	Road	Soil	Water	Tree	Average
CNNAEU	0.584	0.521	0.765	0.814	0.652
MITAEU	0.496	0.711	0.919	1.100	0.798
DAEU	0.490	0.661	0.891	1.186	0.807
DAEN	0.729	0.774	0.960	0.990	0.863
SIDAEU	0.476	0.806	0.904	1.121	0.827
OSPAEU	0.497	0.537	0.852	1.388	0.819

D. Results

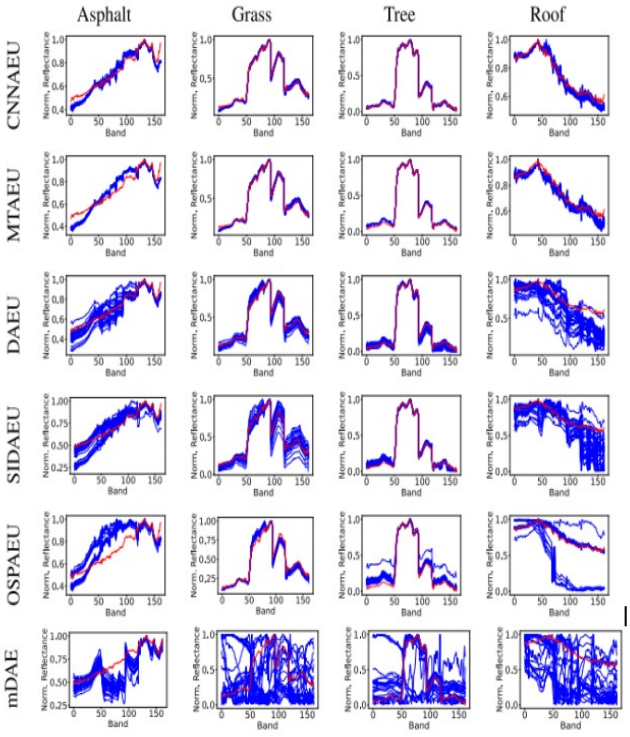

Fig. 1: Endmembers of Urban dataset(4 endmembers)

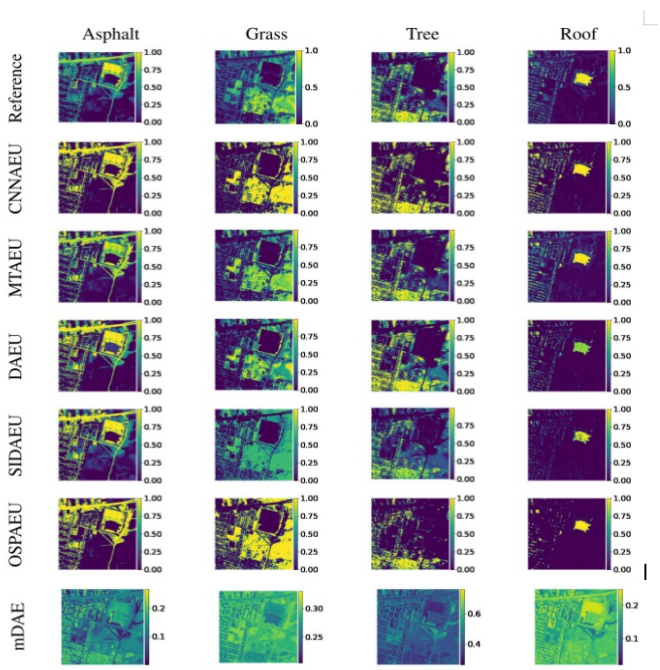

Fig. 2: Abundances of Urban dataset(4 endmembers)

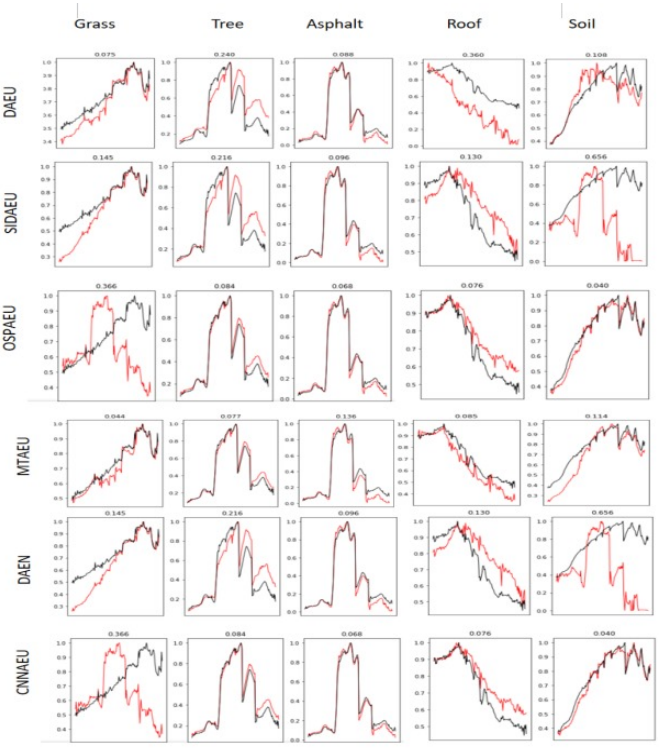

Fig. 3: Endmembers of Urban dataset(5 endmembers)

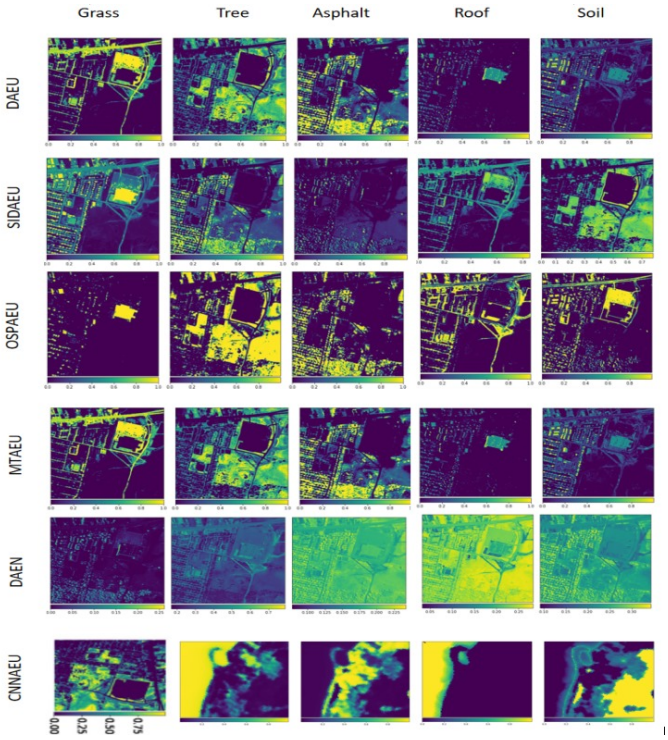

Fig. 4: Abundances of Urban dataset(5 endmembers)

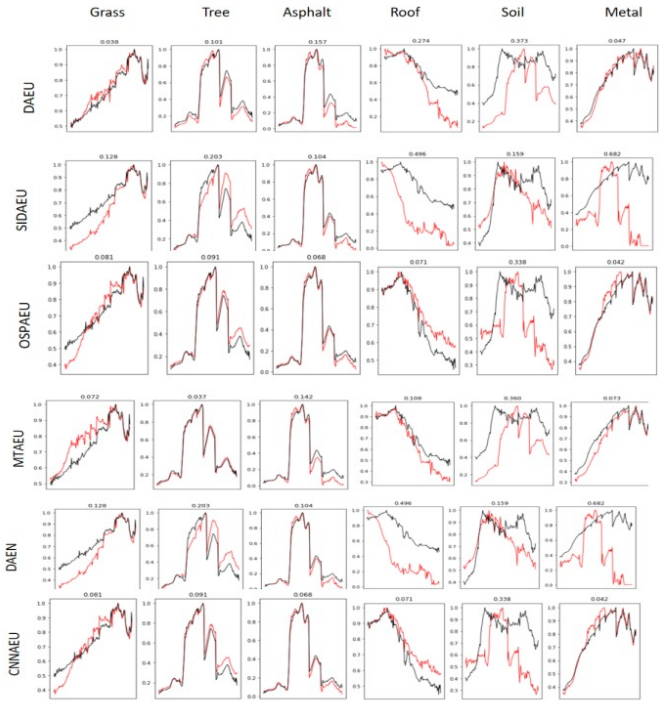

Fig. 5: Endmembers of Urban dataset(6 endmembers)

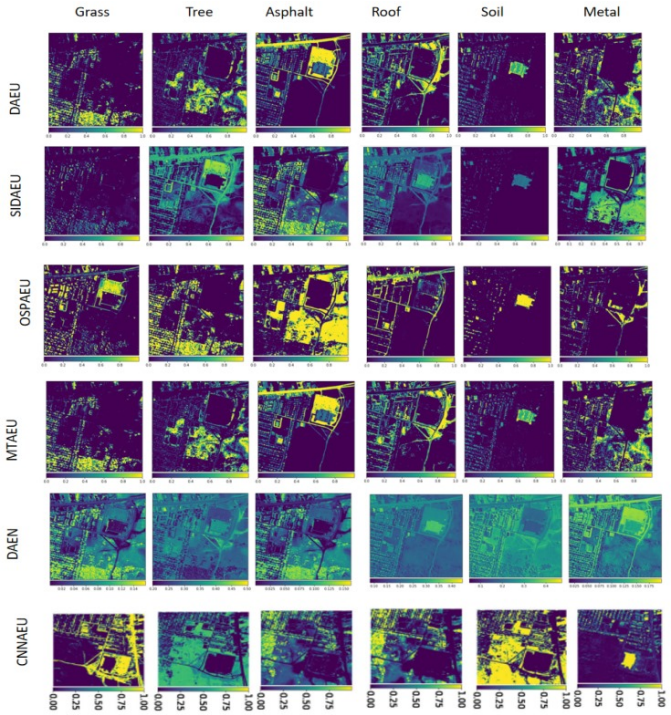

Fig. 6: Abundances of Urban dataset(6 endmembers)

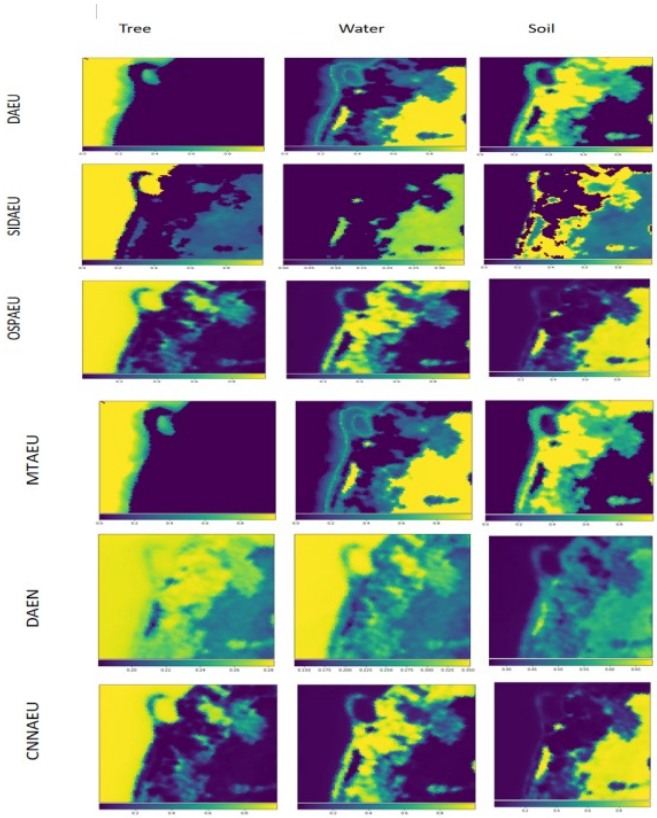

Fig. 8: Abundances of Samson dataset

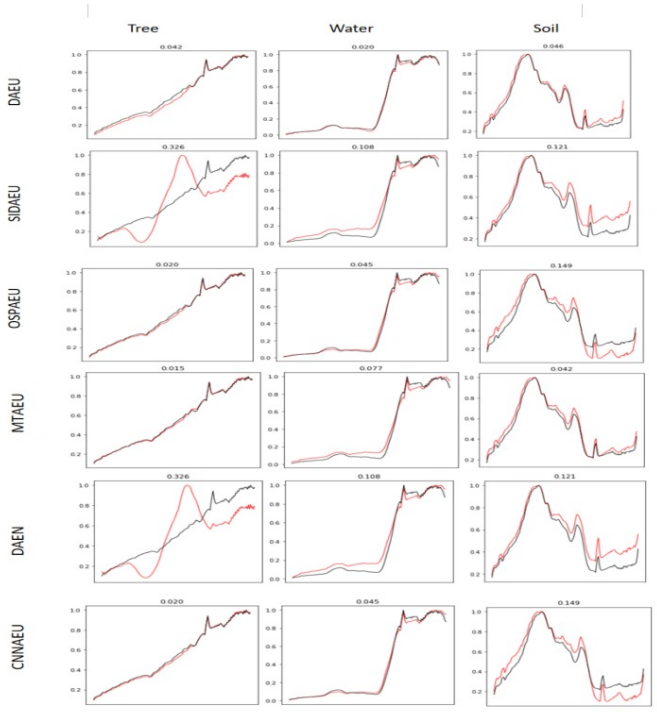

Fig. 7: Endmembers of Samson dataset

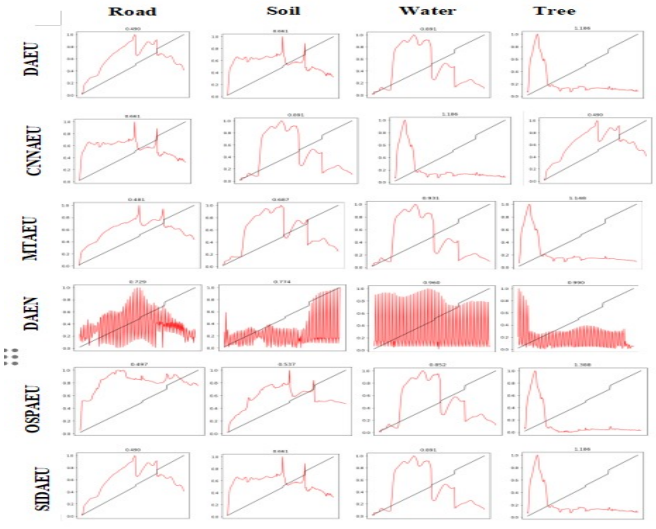

Fig. 9: Endmembers of Jasper Ridge dataset

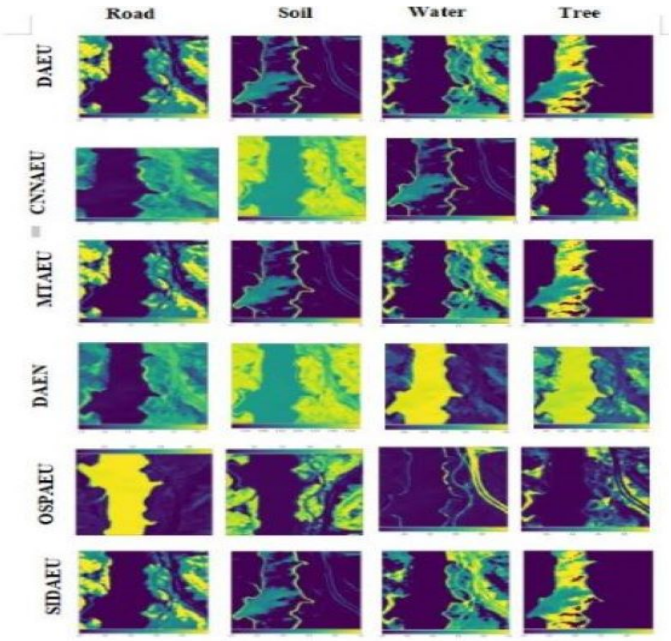

Fig. 10: Abundances of Jasper Ridge dataset

V. Conclusion and future scope

In this study, we investigated the effectiveness of deep and shallow autoencoders combined with six deep unmixing algorithms for extracting endmembers and abundances from hyperspectral pictures. Our analysis included convolutional neural networks (CNN), denoising unmixing, MTAEU, and other pertinent approaches. The performance was evaluated using two criteria: reconstruction error and mean spectral angular difference. The reconstruction error compares the fidelity of the reconstructed hyperspectral image to the original, whereas the mean spectral angular difference quantifies the difference between the estimated and ground truth abundances.

Our findings show that the choice of autoencoder architecture has a considerable impact on the accuracy of endmember extraction and abundance estimation. Deep autoencoders outperformed shallow versions, owing to their ability to capture subtle spectral characteristics and spatial relationships. In conclusion, our study sheds light on the efficacy of autoencoder-based methodologies and deep unmixing methods for hyperspectral picture analysis. The comparison of reconstruction error and mean spectral angular difference provides useful information for researchers and practitioners in selecting appropriate methodologies for their particular applications, furthering the field of hyperspectral image processing and analysis.

Looking ahead, there are a lot of exciting new directions that hyperspectral image analysis can go in. Integrating machine learning methods with domain-specific expertise is a crucial step toward improving the interpretability and generalizability of abundance estimation and endmember extraction [10]. Prior knowledge of spectral signatures, spatial linkages, and material physical qualities can be included to improve current algorithms and enable more precise and perceptive analysis. Furthermore, the utilisation of novel paradigms like transfer learning and self-supervised learning presents opportunities to tackle issues pertaining to insufficient labeled data and domain adaptation. This will facilitate the creation of more resilient and adaptable models that can effectively manage a range of hyperspectral imaging scenarios.

Moreover, the efficiency and scalability of deep unmixing algorithms and autoencoder-based techniques offer prospects for their implementation in real-time or resource-limited settings, such unmanned aerial vehicle (UAV) platforms and remote sensing applications. Large-scale hyperspectral dataset processing can be made easier and more efficient on the fly by streamlining computing procedures, optimizing model designs, and utilizing hardware accelerators. Furthermore, cooperative analysis and scalable deployment across geographically separated locations can be made possible by the integration of these approaches with cloud-based infrastructures and distributed computing frameworks, which promotes cooperation and information sharing in interdisciplinary study fields. Advances in machine learning, signal processing, and remote sensing technologies have the potential to push the limits of hyperspectral picture analysis and provide fresh perspectives on Earth's surface and beyond in the future.

Acknowledgments

The work reported in this paper is supported by the Department of Information Technology of Vasavi College of Engineering, Hyderabad, Telangana, India and we sincerely thank the Department for providing the IBM Power9 deep learning server with access to IBM Power AI Framework for experimentation.

References

[1] B. Luo, J. Chanussot, S. Douté, and L. Zhang, "Empirical automatic estimation of the number of endmembers in hyperspectral images," *IEEE Geoscience and Remote Sensing Letters*, vol. 10, no. 1, pp. 24–28, 2012.

[2] M.-D. Iordache, J. M. Bioucas-Dias, and A. Plaza, "Sparse unmixing of hyperspectral data," *IEEE Transactions on Geoscience and Remote Sensing*, vol. 49, no. 6, pp. 2014–2039, 2011.

[3] M. Wang, M. Zhao, J. Chen, and S. Rahardja, "Nonlinear unmixing of hyperspectral data via deep autoencoder networks," *IEEE Geoscience and Remote Sensing Letters*, vol. 16, no. 9, pp. 1467–1471, 2019.

[4] J. Masci, U. Meier, D. Cireşan, and J. Schmidhuber, "Stacked convolutional auto-encoders for hierarchical feature extraction," in *Artificial Neural Networks and Machine Learning–ICANN 2011: 21st International Conference on Artificial Neural Networks, Espoo, Finland, June 14-17, 2011, Proceedings, Part I 21*. Springer, 2011, pp. 52–59.

[5] R. Heylen, M. Parente, and P. Gader, "A review of nonlinear hyperspectral unmixing methods," *IEEE Journal of Selected Topics in Applied Earth Observations and Remote Sensing*, vol. 7, no. 6, pp. 1844–1868, 2014.

[6] J. M. Bioucas-Dias, A. Plaza, N. Dobigeon, M. Parente, Q. Du, P. Gader, and J. Chanussot, "Hyperspectral unmixing overview: Geometrical, statistical, and sparse regression-based approaches," *IEEE journal of selected topics in applied earth observations and remote sensing*, vol. 5, no. 2, pp. 354–379, 2012.

[7] A. Zare and K. Ho, "Endmember variability in hyperspectral analysis: Addressing spectral variability during spectral unmixing," *IEEE Signal Processing Magazine*, vol. 31, no. 1, pp. 95–104, 2013.

[8] B. Somers, G. P. Asner, L. Tits, and P. Coppin, "Endmember variability in spectral mixture analysis: A review," *Remote Sensing of Environment*, vol. 115, no. 7, pp. 1603–1616, 2011.

[9] L. J. Rickard, R. W. Basedow, E. F. Zalewski, P. R. Silverglate, and M. Landers, "Hydice: An airborne system for hyperspectral imaging," in *Imaging Spectrometry of the Terrestrial Environment*, vol. 1937. SPIE, 1993, pp. 173–179.

[10] T. D. McRae, D. Oleksyn, J. Miller, and Y.-R. Gao, "Robust blind spectral unmixing for fluorescence microscopy using unsupervised learning," *Plos one*, vol. 14, no. 12, p. e0225410, 2019.